Applied Catalysis B: Environmental 327 (2023) 122431

Contents lists available at ScienceDirect

Applied Catalysis B: Environmental

journal homepage: www.elsevier.com/locate/apcatb

Hydrogen evolution and electric power generation through photoelectrochemical oxidation of cellulose dissolved in aqueous solution

Yosuke Kageshima [a,b,*], Hiromasa Wada [a], Katsuya Teshima [a,b], Hiromasa Nishikiori [a,b,*]

[a] Department of Materials Chemistry, Faculty of Engineering, Shinshu University, 4–17-1 Wakasato, Nagano 380–8553, Japan
[b] Research Initiative for Supra-Materials (RISM), Shinshu University, 4–17-1 Wakasato, Nagano 380–8553, Japan

ARTICLE INFO

Keywords:
Photoelectrochemical cell
Biomass
Cellulose
Hydrogen evolution
Electric power generation

ABSTRACT

Photoelectrochemical (PEC) cells capable of generating electricity or hydrogen through the oxidation of cellulose dissolved in an aqueous solution were constructed. As distinct from solid cellulose, the cellulose liquid fuel was beneficial for enabling a continuous reactant supply. Product analyses revealed that the cellulose macromolecules were cleaved to small organic acids and finally decomposed to CO_2. During the electricity generation, the maximum power density of the PEC cell reached 1.13 mW cm^{-2}. The influence of the photoelectrode structure on the PEC performance was elucidated. The monolithic structure of photoanodes consisting of an approximate monolayer of $SrTiO_3$ particles anchored onto the backside metal layer provided a high photocurrent during oxygen evolution. The porous photoanode composed of heavily stacked TiO_2 nanoparticles was found to be suitable for cellulose decomposition because of the high specific surface area. The present study should serve as a foundation for the direct energy utilization of waste biomass.

1. Introduction

Renewable energies such as solar and biomass represent promising alternatives to fossil fuels. In particular, cellulose, which accounts for a large fraction of waste biomass, is a potential unharnessed resource. Because typical biomass reforming processes (*e.g.*, thermal decomposition, saccharification, and fermentation) require substantial energy inputs [1–3], the direct utilization of cellulose as a fuel would be preferable. As a potential technology for chemical production or electric power generation directly from cellulose, photocatalytic and photoelectrochemical (PEC) reforming of cellulose have been investigated [4–12]. Most of the previous studies involving photocatalytic and PEC reforming of biomass-related compounds have used low-molecular-weight organics, presumably derived from advance reforming of biomass, as the electron donor [13,14]. The direct photocatalytic and PEC reforming of cellulose should contribute to the energy-saving and simplification of the overall energy conversion system. However, because cellulose is insoluble in almost all solvents, almost all of the previously related studies have used "solid" cellulose as a reaction substrate (*e.g.*, an aqueous "dispersion" of particulate cellulose). When used as a fuel, solid cellulose hampers the continuous supply of reactant to the photocatalytic system as well as the separation of catalysts from reaction residues, impeding its future industrial implementation. For instance, we have reported that a PEC cell consisting of a TiO_2 photoanode coated with a cellulose solid thin film can generate electricity with oxidization of the solid cellulose [8]. Such PEC cells are intended to boost the power generation efficiency from biomass by combining the energy of light. However, the photocurrent generated by the PEC cell was inactivated within only 30 min because of rapid consumption of the solid cellulose.

Cellulose can be well dissolved in strongly alkaline aqueous solutions (*e.g.*, 2 M NaOH) by the freezing method [15–17], and the resultant solutions have thus been used as a "liquid" fuel for direct cellulose fuel cells (DCFCs) [18–20]. Compared with solid cellulose, cellulose in the form of liquid fuel is preferable for achieving a continuous supply of reactant to an energy conversion device as well as for promoting reactant diffusion at the microscale. In addition, solubilization of cellulose might make more cellulose available for fuel, even in a batch cell. Although cellulose can be dissolved in other special solvents such as ionic liquids or highly concentrated metal salt solutions—indeed, a few cases of the photocatalysis of cellulose dissolved in a metal salt hydrate have been reported [21]—undesirable side reactions related to the solvent itself or to metal salts, as well as difficult handling of the special solvents, are serious concerns. NaOH solution, a relatively clean and

* Corresponding authors at: Department of Materials Chemistry, Faculty of Engineering, Shinshu University, 4–17-1 Wakasato, Nagano 380–8553, Japan.
E-mail addresses: kage_ysk@shinshu-u.ac.jp (Y. Kageshima), nishiki@shinshu-u.ac.jp (H. Nishikiori).

https://doi.org/10.1016/j.apcatb.2023.122431
Received 26 October 2022; Received in revised form 13 January 2023; Accepted 2 February 2023
Available online 4 February 2023

manageable aqueous solution that is commonly used as an electrolyte in photocatalysis and PEC reactions, is preferable. However, to our knowledge, the literature contains no reports of such a "simple" cellulose aqueous solution for photocatalysis and photoelectrocatalysis.

In the present study, we evaluated the PEC performance of a particulate TiO_2 photoanode during oxidation of cellulose dissolved in a strongly alkaline aqueous solution. We demonstrated that, by combining the oxygen reduction reaction (ORR) or hydrogen evolution reaction (HER) as a cathodic reaction on a Pt-based cathode, the PEC cell generated electricity in an external circuit or produced H_2 spontaneously, respectively. In addition, we elucidated the influence of the photoelectrode structure on the PEC performance using TiO_2 and $SrTiO_3$ (STO) particles as model photocatalysts to deduce future guidelines for designing an efficient photoanode intended for cellulose oxidation. The monolithic structure of the photoanode, where an approximate monolayer of photocatalytic particles was directly anchored onto the backside metal electrode, was prepared *via* the particle transfer (PT) method [22], whereas the porous photoanode composed of stacked photocatalytic particles was obtained by coating a multilayer of photocatalytic particles onto a transparent conductive substrate. The PEC performances of the TiO_2 and STO particulate photoanodes with different structures during the oxygen evolution reaction (OER), methanol oxidation, and cellulose oxidation were comprehensively compared.

2. Experimental section

2.1. Electrolyte preparation

A cellulose aqueous solution was prepared by a freezing method described elsewhere [15–20]. Particulate microcrystalline cellulose (average molecular weight: 40,000; average aspect ratio: 10; diameter: 1–10 μm) equivalent to 0.15 M glucose units (referred to simply as 0.15 M cellulose) was well dispersed in 2 M NaOH solution in a perfluoroalkoxy alkane (PFA) bottle. The cellulose aqueous dispersion was then frozen by immersing the PFA bottle into liquid N_2. After the specimen was thawed at 313 K, a transparent and slightly viscous aqueous solution was obtained. A Debye plot for the cellulose solution was constructed by assuming the differential refractive index value (dn/dc) was 0.1 [23,24]; the result is presented in Fig. S1 in the Supporting Information (SI). The molecular weight of the cellulose dissolved in the NaOH solution was roughly estimated to be 32,230. The similarity in molecular weight between the liquid-phase and solid reagents implies that a large portion of the cellulose was dissolved in the solution in the form of macromolecules rather than as low-molecular-weight compounds derived from the hydrolysis of cellulose. For assessment of the OER performance, a 2 M NaOH solution was used as an electrolyte. In the case of methanol oxidation, a 2 M NaOH solution containing 0.15 M methanol was used as an electrolyte.

2.2. Preparation of photoelectrodes

Four types of particulate photoanodes (TiO_2 stacked, STO stacked, TiO_2 PT, and STO PT photoanodes) were prepared as follows. For fabrication of TiO_2 stacked photoanodes, a fluorine-doped thin oxide-coated glass (FTO/glass) substrate was sequentially cleaned with acetone, ethanol, and water and then coated with a TiO_2 thin film by the sol–gel method. A paste containing commercially available TiO_2 particles (Aerosil AEROXIDE, P25) was deposited using a squeegee method onto the FTO/glass substrate coated with a TiO_2 sol–gel thin film, and the resultant specimen was calcined at 723 K for 30 min, resulting in a porous photoanode. The details are described elsewhere [8]. STO stacked photoanodes were also fabricated in a similar manner, where STO particles synthesized *via* a solid-state reaction [25,26] were deposited onto the FTO/glass substrate coated with a TiO_2 sol–gel thin film by drop-casting the suspension, followed by a necking treatment using $TiCl_4$ and subsequent calcination at 723 K for 30 min. For fabrication of TiO_2 PT photoanodes, P25 TiO_2 particles were coated onto the glass substrate by spray-coating a suspension of the particles in isopropanol, followed by drying in air and calcination at 723 K for 30 min. A thin Ta contact layer and subsequent thick Ti conductor layer were deposited onto the particles using radio-frequency magnetron sputtering. During the sputtering process, the temperature of the TiO_2-coated primary glass substrate was maintained at 573 K. The composite of TiO_2 particles anchored on the metal layer served as a photoanode after it was fixed onto a secondary glass substrate using carbon tape and the excess particles were removed by sonication. STO PT photoanodes were also prepared using the PT method, where STO particles were deposited onto the primary glass substrate by drop-casting, followed by drying in air, deposition of a metal layer by sputtering, transfer of the metal layer to the secondary glass substrate, and removal of the excess particles. Schematics of the fabrication process of the stacked and PT photoanodes are provided in Fig. S2. The basic physical characteristics (X-ray diffraction (XRD) patterns and diffuse-reflectance (DR) spectra) of the photocatalytic particles used in the present study are presented in Fig. S3. Pt catalysts for the ORR were deposited onto a Ni foam substrate (with a geometric size of approximately 1.3×1.8 cm^2) by a sputtering method, and the loaded substrate, referred to as Pt/Ni foam, was used as the cathode.

2.3. Photoelectrochemical measurements

The PEC measurements were conducted using a typical three-electrode configuration, whereas the photovoltaic or H_2 production performances were evaluated under a two-electrode setup. The particulate photoanode, the Pt-based cathode, and a commercially available reversible hydrogen electrode (RHE) were used as the working, counter, and reference electrodes, respectively. For the assessment of the stacked photoanodes, a two-chamber cell divided by a membrane filter as described in Fig. S4a was used, where the photoanode composed of FTO/glass substrate itself was equipped as a window and irradiated from the glass-substrate side. The area of photoanode exposed to the electrolyte and irradiated by light was 1.0 cm^2. During the PEC measurements in a two-electrode configuration, the same two-chamber cell used for the three-electrode measurements (Fig. S4a) was employed, where the reference electrode was removed and the photoanode and cathode were connected in a two-electrode configuration. In the case of the PT photoanodes, because the PT photoanodes were not transparent and therefore could not be irradiated from the substrate side, a different configuration of the two-chambered PEC cell was used (Fig. S4b). In this case, the PT photoanode was irradiated from the photocatalyst side through the electrolyte. The cellulose solution, methanol solution, and NaOH solution purged with Ar were loaded into the anolyte during cellulose oxidation, methanol oxidation, and the OER, respectively. The catholyte was filled with 2 M NaOH, which was bubbled with O_2 or Ar during the ORR or HER as a cathodic reaction, respectively. The electrolytes were vigorously stirred during the measurements. A 300 W Xe lamp equipped with a cold mirror ($\lambda < 500$ nm) was used as a light source. Spectra of the light sources used in the experiments are provided in Fig. S5.

2.4. Product analyses

The organic acids dissolved in the anolyte after the PEC reaction were identified using high-performance liquid chromatography (HPLC) [8,18]. The residual cellulose was first removed from the electrolyte by neutralizing the electrolyte with aqueous HCl, followed by removal of the solid precipitate by centrifugation. The neutralized electrolyte was then filtered through a hydrophilic nylon filter with a 0.22 μm pore size to remove fine particles, and 20 μL of the specimen was injected into an HPLC system (Shimadzu, Shimadzu Prominence LC-20A) equipped with an ultraviolet–visible (UV–vis) detector (Shimadzu, SPD-20A) and a Rezex RHM-Monosaccharide column (Phenomenex, HPX-87 H, 300 ×

7.8 mm^2). The column temperature was maintained at 333 K, and an aqueous 4 mM H_2SO_4 solution was used as the eluent at a flow rate of 0.8 mL min^{-1}. The residual cellulose regenerated as a solid by neutralization using HCl was pressed into KBr pellets and characterized using Fourier transform infrared (FTIR) spectroscopy (Shimadzu, IRPrestige-21). The CO_2 dissolved in the strongly alkaline electrolyte after the PEC reaction was quantified on the basis of the membrane electrode method using a commercial CO_2 concentration meter (Dkk-Toa, CGP-31). In these trials, the pH of the electrolyte was adjusted to be less than 4 by adding aqueous HCl immediately before the CO_2 concentration was measured. Gaseous products (*i.e.*, H_2 and O_2) were quantified using a gas chromatograph (Agilent, 990 Micro GC) connected to a batch-type gas-tight PEC cell; Ar was used as the carrier gas (Fig. S6). A Ag/AgCl electrode in saturated KCl was used as a reference electrode instead of an RHE. Notably, the stacked TiO_2 photoanode was irradiated from the glass-substrate side through the layer of the electrolyte only during the gas analyses because of limitations imposed by the cell configuration. During the PEC measurements in a two-electrode configuration, the same batch-type gas-tight cell was used with the reference electrode removed.

2.5. Characterization

The morphology of the particulate photoanodes was examined by scanning electron microscopy (SEM; Hitachi, SU8000). The transmittance spectra of the electrolytes and DR spectra of the particulate materials were acquired using a UV–vis–near-infrared spectrophotometer (Jasco, V-770). The crystalline structures of the photocatalytic particles were characterized by XRD (Rigaku, MiniFlex600) using Cu Kα radiation.

3. Results and discussion

3.1. Construction of photoelectrochemical cells for electric power generation or hydrogen production

The current–potential curves for the TiO_2 stacked photoanode in NaOH electrolyte with and without cellulose solute, as measured in a three-electrode configuration, are shown in Fig. 1a. The anodic photocurrent was observed at a potential more positive than − 0.21 and 0.015 V_{RHE} when cellulose was present and absent, respectively. The anodic photocurrent generated by the TiO_2 stacked photoanode gradually increased according to the applied positive potential and reached 6.7 and 3.8 mA cm^{-2} at 1.0 V_{RHE} when cellulose was present and absent, respectively. The photocurrent observed in the cellulose solution is likely derived from cellulose oxidation, whereas the OER should proceed in the electrolyte without cellulose. (Detailed product analyses are discussed in the next section.) The addition of cellulose as a liquid fuel apparently enhanced the PEC performance of the TiO_2 stacked photoanode; that is, it induced a negative shift of the onset potential and increased the photocurrent at positive potentials because the cellulose oxidation is thermodynamically preferred compared with the OER [8].

The electrocatalytic performance of the Pt/Ni foam cathode during the ORR and HER is also shown in Fig. 1a. The Pt/Ni foam in NaOH solution bubbled with O_2 generated a cathodic current originating from the ORR at a potential more negative than 0.93 V_{RHE}. The onset potential of the Pt/Ni foam cathode during the ORR was more positive than 1 V above the onset potential of TiO_2 for cellulose oxidation, and the cathode and photoanode could generate current at the same potential. This overlapping of current–potential curves indicates that the PEC cell consisting of a TiO_2 stacked photoanode and a Pt/Ni foam cathode on which the cellulose oxidation and ORR reactions occur, respectively, can be expected to generate electricity in the external circuit under light irradiation. Meanwhile, the Pt/Ni foam in NaOH solution purged with Ar showed a HER onset potential of ~0.15 V_{RHE}. Notably, a cathodic current was observed at potentials more positive than 0 V_{RHE} because the electrolyte was purged with Ar. Although the current–potential curve of a TiO_2 stacked photoanode in NaOH solution without cellulose showed almost negligible overlap with that of the Pt/Ni foam during the HER, the TiO_2 with cellulose and the Pt/Ni foam during HER exhibited an obvious overlap at − 0.036 V_{RHE}. This result indicates that the present PEC cell should be capable of driving spontaneous cellulose oxidation and H_2 evolution without an external bias voltage but should be almost inactive toward overall water splitting into H_2 and O_2.

The stability of the photocurrent generated by the TiO_2 stacked photoanode was assessed at a constant applied potential of 0 V_{RHE} (Fig. 1b). The results obtained using the TiO_2 stacked photoanode loaded with a solid cellulose thin film as a fuel are included in Fib. 1b for comparison [8]. As we have already reported, the photocurrent generated from the solid cellulose gradually decreased over time, reaching a photocurrent similar to that of the bare TiO_2, possibly because of rapid consumption of the solid cellulose fuel directly attached to the TiO_2 surface. Meanwhile, the TiO_2 stacked photoanode in the cellulose solution exhibited a stable anodic photocurrent for 3 h under light illumination. The stable generation of a photocurrent is attributable to the continuous supply of reactant to the photoanode from the bulk of the liquid phase. Here, a continuous supply of cellulose suspension to the PEC device itself might be possible. However, we found that the particulate solid cellulose can easily precipitate within a few minutes without any stirring or convection (Fig. S7). Supply of the fuel dispersion to the flow-type PEC device thus might lead to clogged flow paths. In addition, we also considered that cellulose dissolved in a liquid phase

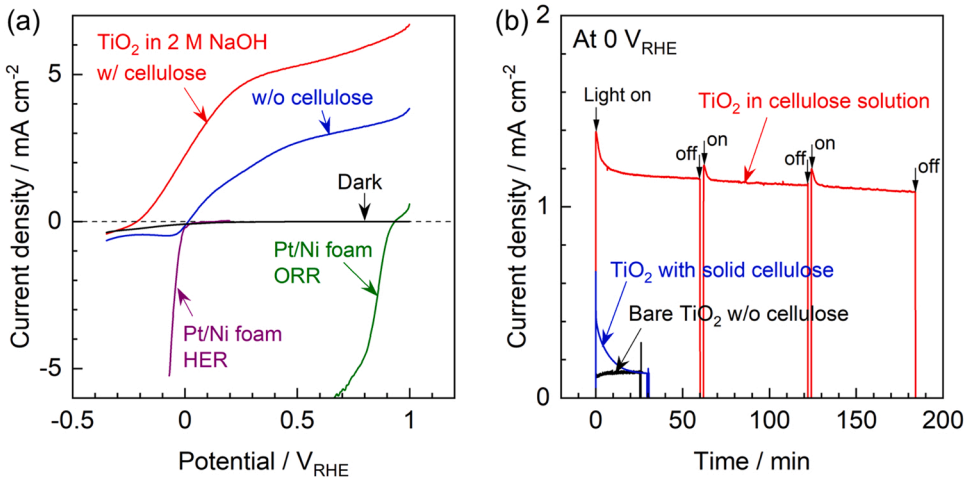

Fig. 1. (a) Current–potential curves of a TiO_2 stacked photoanode in cellulose aqueous solution and 2 M NaOH solution (without cellulose). Current–potential curves of a Pt/Ni cathode during the ORR and HER are also shown. (b) Current–time curves of a TiO_2 stacked photoanode in cellulose aqueous solution and the photoanode coated with solid cellulose in 0.1 M NaOH solution under an applied potential of 0 V_{RHE}. Results for a bare TiO_2 stacked photoanode (without solid or liquid cellulose as a fuel) in 0.1 M NaOH are also presented. A 300 W Xe lamp ($\lambda < 500$ nm) was used as a light source.

should promote reactant diffusion at the microscale compared with the solid dispersion. The electrochemical measurements revealed that, in the case of the cellulose dispersion, the reactant supply from the bulk electrolyte to the active sites at the microscale should be governed by natural convection flow rather than by diffusion driven by concentration gradients (Fig. S8). Other possibilities are that the solid cellulose particles exhibit low reactivity because of their limited surface area and that the concentration of cellulose derivatives dissolved from the solid cellulose into the aqueous dispersion is low compared with the concentration of the cellulose solution. As a result of poor reactant supply at the microscale (diffusion) and/or low reactivity of the cellulose dispersion, the anodic photocurrent generated by a stacked TiO_2 photoanode in the dispersion was obviously smaller than that generated by the same electrode in the cellulose solution (Fig. S9). These observations strongly demonstrate the superiority of using a cellulose solution as a fuel rather than solid cellulose.

The PEC cell consisting of the TiO_2 stacked photoanode in cellulose solution and a Pt/Ni foam cathode in NaOH solution bubbled with O_2 in a two-electrode configuration generated electricity with a 1.1 V open-circuit voltage (V_{OC}) and a 5.0 mA cm^{-2} short-circuit current density (I_{SC}) (Fig. 2a). The addition of cellulose as a fuel substantially enhanced the PEC performance compared with that of the PEC cell without cellulose, where the electric power generated was derived from the redox reactions of O_2 (OER at the photoanode and ORR at the cathode) (Fig. 2a). The observed current–voltage profile agrees well with each current–potential curve recorded using a three-electrode setup. The present PEC cell generated a V_{OC} substantially greater than that generated by DCFCs [18–20] and other typical fuel cells that use organic fuels [27–31] because of the assistance by the energy of light. Here, the reaction mechanisms occurring during electrochemical and PEC cellulose oxidation should differ. That is, the cellulose macromolecules are gradually cleaved into short hydrocarbons during the electrochemical reaction [18], whereas cellulose is completely decomposed into CO_2 during the PEC reaction, as discussed in a later section. However, the V_{OC} of the (photo)electrochemical cells in the two-electrode configuration is predominantly governed by the difference between the onset potentials for the anode and cathode, irrespective of whether the reaction substrate is partially or fully oxidized. Therefore, this performance gain is achieved because the thermodynamically expected photovoltage for the PEC cell is determined by the difference between the flat-band potential of the photoanode and the equilibrium potential for the ORR, whereas the maximum V_{OC} expected for a typical fuel cell reflects the difference between the organic decomposition potential and the ORR potential. The power density–voltage profile of the PEC cell (Fig. S10) shows that the maximum power density reached 1.13 mW cm^{-2}. Notably, the electrocatalytic performance of the present Pt/Ni foam cathode during the ORR was not as high as that of state-of-the-art electrocatalysts [32]. A possible reason for the low electrocatalytic performance of the Pt/Ni foam is sluggish mass transfer through the foam structure. Another possibility is that the small size of the catholyte chamber and the long distance between the photoanode and cathode (Fig. S4a) caused a decrease in the overall PEC cell performance in the two-electrode configuration. Nevertheless, the ORR performance of the cathode and the efficiency of the device in the two-electrode configuration can be improved in the future by replacing the Pt/Ni foam with a more efficient cathode as well as by designing a more appropriate cell.

The current–voltage profile during H_2 evolution was also

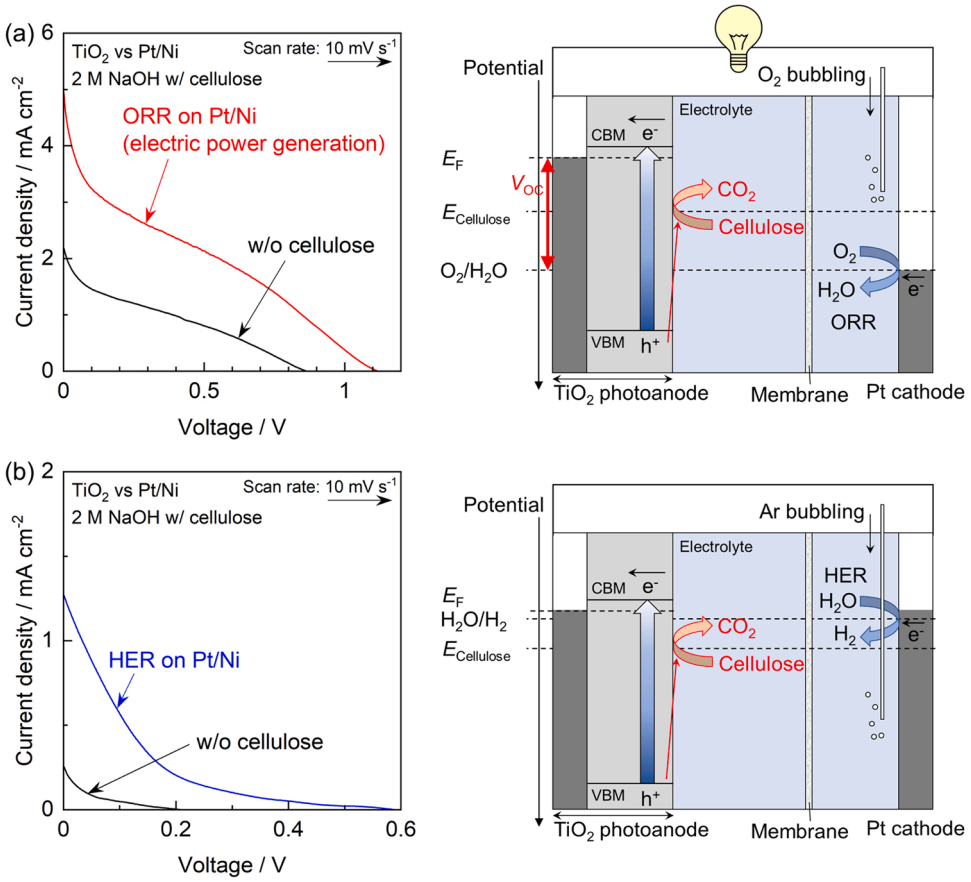

Fig. 2. Current–voltage profiles of the PEC cell consisting of a TiO_2 stacked photoanode and a Pt/Ni foam cathode in a two-electrode configuration in 2 M NaOH solution with and without cellulose (a) during electric power generation and (b) during H_2 evolution under illumination with a 300 W Xe lamp ($\lambda < 500$ nm). Schematics corresponding to the cathode performing the ORR or HER are also shown.

characterized (Fig. 2b). The PEC cell consisting of the TiO_2 stacked photoanode in cellulose solution and the Pt/Ni foam cathode in NaOH solution purged with Ar in a two-electrode configuration exhibited a photocurrent of 1.3 mA cm^{-2} under the short-circuit condition, consistent with the results obtained in a three-electrode configuration. The H_2 evolution rate from cellulose solution was substantially greater than the rate of overall water splitting (*i.e.*, the stoichiometric generation of H_2 and O_2) using the TiO_2 stacked photoanode (Fig. 2b). This result indicates that the PEC cell should be capable of H_2 evolution from a cellulose solution *via* a one-step photoexcitation process in the absence of an applied bias. We concluded that we had constructed a PEC cell that converts the energy of cellulose and light into electricity or H_2. Here, we compared the performance of the proposed PEC cell with that of cells reported in relevant studies involving PEC and photocatalytic biomass reforming, as summarized in Table S1 [5,7,8,13,14,33–37]. The performance of the proposed PEC cell using the cellulose solution is comparable to that of previously reported cells. Moreover, most of the previous studies used low-molecular-weight biomass (cellulose derivatives) or solid cellulose as a reaction substrate, supporting the novelty of the present approach using a cellulose aqueous solution as a liquid fuel. Meanwhile, the proposed PEC cell certainly demonstrated electric power generation and H_2 evolution even under simulated sunlight (Fig. S11). However, the efficiency of the PEC cell appears to be insufficient for practical industrial applications because TiO_2 can absorb only UV light. The freezing method used in the present study to prepare the cellulose solution actually requires additional energy input (low temperatures). To compensate for this energy expenditure, improving the PEC cell efficiency is indispensable. One possible approach to improving the efficiency of the PEC cell is to use visible-light-responsive photoanodes (*e.g.*, $BiVO_4$, WO_3, and CdS). However, typical visible-light-responsive photoanode materials usually suffer from instability in strongly alkaline solutions (2 M NaOH in the present case). Therefore, protection and stabilization of such photoanode materials against harsh alkaline conditions are important future challenges.

3.2. Product analyses and reaction mechanisms during cellulose oxidation

To elucidate the reaction pathway during PEC cellulose oxidation, the time courses of the generation of water-soluble organic acids were characterized using HPLC (Fig. 3a). Typical chromatograms and the time courses at different applied potentials are summarized in Figs. S12 and S13, respectively. The cellulose solution before the PEC reaction already contained small amounts of some carboxylic acids, indicating that the dissolution of cellulose into the highly alkaline solution involved some degree of hydrolysis of the cellulose skeleton between glucose units and intramolecular decomposition of the glucose derivatives [18]. Under prolonged light illumination, the concentrations of organic acids—especially short-chain carboxylic acids such as formic acid, malonic acid, and glyceric acid—obviously increased. The generation rate of the organic acids also increased when a potential was applied (Fig. S13c). These observations are consistent with our previously reported results of product analyses during the PEC oxidation of solid cellulose [8] and during the electrochemical oxidation of cellulose in a liquid [18]. In addition, FTIR spectra of the residual cellulose indicated hydrolysis of the cellulose skeleton in the liquid after the PEC reaction (Figs. S14–S16), consistent with our previous report regarding the electrocatalysis of cellulose solutions [18,31–41]. Therefore, we speculated that the hydrolysis of the cellulose skeleton and the decomposition of the glucose derivatives would be promoted by the PEC process. However, the concentrations of glycolic acid, malonic acid, and

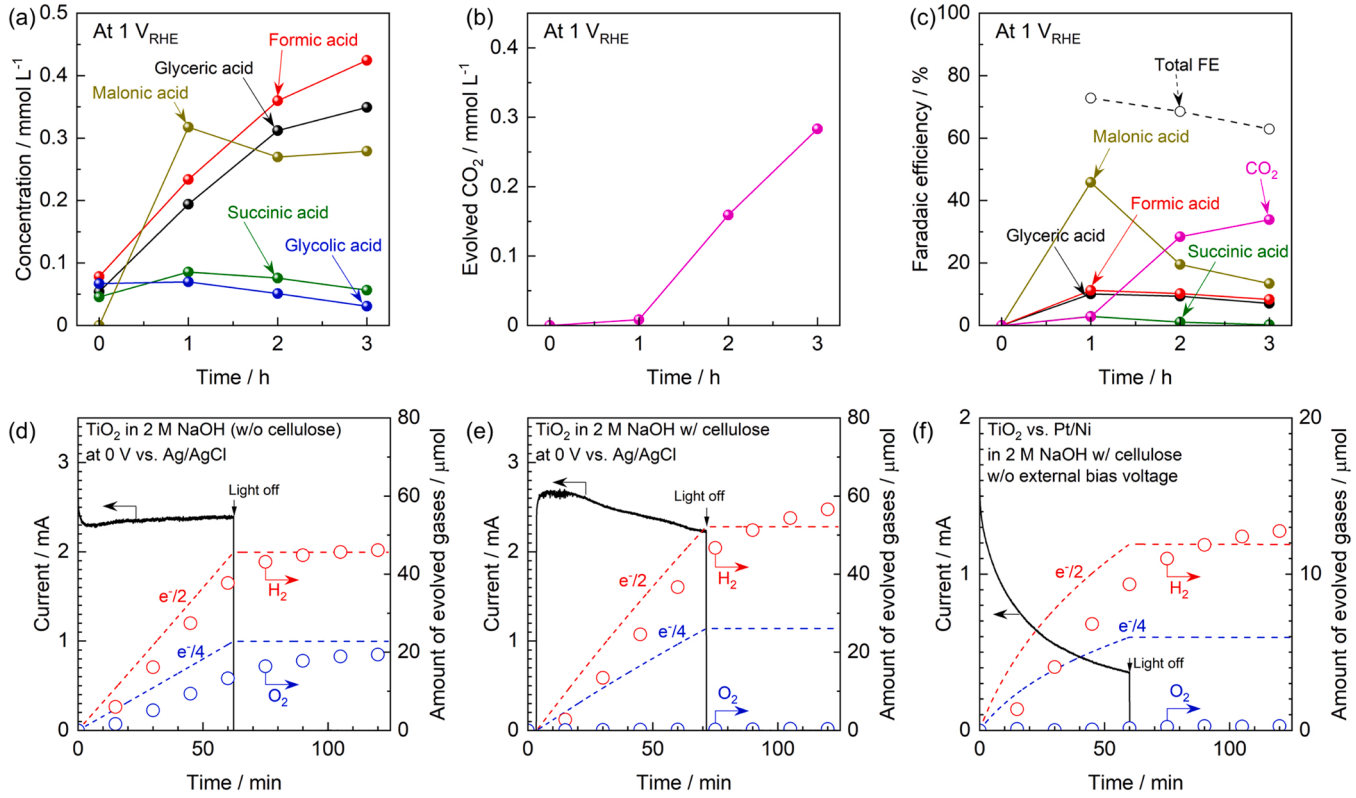

Fig. 3. (a and b) Time courses of (a) organic acids determined by HPLC and (b) evolved CO_2 quantified by a membrane electrode during PEC cellulose oxidation using a TiO_2 stacked photoanode in a cellulose aqueous solution under an applied potential of 1 V_{RHE}. (c) The corresponding FEs for the production of the organic acids and CO_2. (d and e) Time courses of the photocurrent, expected yield of evolved H_2 and O_2 calculated as $e^-/2$ and $e^-/4$, respectively, and the actual amounts of evolved H_2 and O_2 determined by GC using (d) the TiO_2 stacked photoanode in 2 M NaOH without cellulose and (e) the photoanode in cellulose aqueous solution under an applied potential of 0 V *vs.* Ag/AgCl. (f) Time course of H_2 evolution using the PEC cell consisting of a TiO_2 stacked photoanode and a Pt/Ni foam cathode without any external bias voltage. A 300 W Xe lamp ($\lambda < 500$ nm) was used as a light source.

succinic acid were found to decrease under prolonged light irradiation. If the cellulose and the related intermediates were finally decomposed into CO_2, they should be completely captured in the highly alkaline solution in the form of carbonate rather than in the form of gaseous CO_2. A commercial CO_2 concentration meter was calibrated using $NaHCO_3$ aqueous solutions of various known concentrations, and we confirmed that the presence of cellulose did not affect the sensitivity of the membrane electrode (Fig. S17a). Because CO_2 in air was also gradually dissolved into the strongly alkaline solution even under bubbling with inert gas (Fig. S17b), the difference in the CO_2 concentration between the PEC trial and the control experiment in the absence of cellulose (Fig. S17c) was regarded as the CO_2 that "evolved" through PEC cellulose oxidation (Fig. 3b). The concentration of CO_2 clearly increased under the prolonged light irradiation, indicating that the final product of the PEC cellulose oxidation should be CO_2. The faradaic efficiencies (FEs) corresponding to the conversion of cellulose into the organic acids and CO_2 under alkaline conditions were calculated assuming the following Eqs. (1)–(5); the results are summarized in Fig. 3c.

$$\textit{Succinic acid formation}: (C_6H_{10}O_5)_n + 3nOH^- \rightarrow 1{\cdot}5nC_4H_6O_4 + 2nH_2O + 3ne^- \quad (1)$$

$$\textit{Glyceric acid formation}: (C_6H_{10}O_5)_n + 4nOH^- \rightarrow 2nC_3H_6O_4 + nH_2O + 4ne^- \quad (2)$$

$$\textit{Malonic acid formation}: (C_6H_{10}O_5)_n + 8nOH^- \rightarrow 2nC_3H_4O_4 + 5nH_2O + 8ne^- \quad (3)$$

$$\textit{Formic acid formation}: (C_6H_{10}O_5)_n + 12nOH^- \rightarrow 6nCH_2O_2 + 5nH_2O + 12ne^- \quad (4)$$

$$\textit{CO}_2\textit{ formation}: (C_6H_{10}O_5)n + 36nOH^- \rightarrow 6nCO_3^{2-} + 23nH_2O + 24ne^- \quad (5)$$

Here, we note that OH^- in the electrolyte is consumed during the cellulose oxidation and that the pH of the electrolyte near the photoanode might therefore decrease. However, the cathode reaction (ORR or HER) is accompanied by the production of OH^-; thus, the total pH balance in the PEC cell should be unchanged. During the initial 1 h of light illumination, the TiO_2 stacked photoanode showed a relatively high FE for malonic acid formation: approximately 46%. Under further light illumination, the FE for organic acid formation slightly decreased, whereas the FE for CO_2 generation reached 34% after 3 h of PEC reaction. The total FEs regarding the organic acids that could be assigned in the present trials and CO_2 were approximately 60–70%, suggesting that a large portion of the photogenerated holes were consumed by the cellulose oxidation to CO_2 through organic acid intermediates.

To investigate the possibility of the OER competing against the cellulose oxidation reaction, we also analyzed the gaseous products generated during the PEC reaction. When the TiO_2 stacked photoanode was irradiated under a constant applied potential in the strongly alkaline solution without cellulose, the photoanode and the counter electrode generated stoichiometric amounts of O_2 and H_2 in quantities approximately consistent with the values calculated from the simultaneously recorded current (Fig. 3d). Interestingly, when cellulose was dissolved in the electrolyte, the TiO_2 stacked photoanode generated only a trace amount of O_2 although the counter electrode certainly generated H_2 (Fig. 3e). The corresponding FE for the OER was only 1.5%. These results indicate that almost all the photogenerated holes in the TiO_2 photoanode were involved in the cellulose oxidation without consumption by the OER side reaction. Therefore, the remaining several tens of percent of FEs in Fig. 3c imply the existence of relatively large macromolecules derived from the scission of cellulose chains; these macromolecules could not be detected or assigned on the basis of the HPLC measurement results.

Spontaneous H_2 evolution from the cellulose solution was demonstrated when the PEC cell consisting of the TiO_2 stacked photoanode and the Pt/Ni foam cathode connected in a two-electrode configuration was used without any external bias voltage (Fig. 3 f). The amounts of H_2 evolved were consistent with the expected values calculated from the current passed through the circuit, whereas negligible amounts of O_2 (equivalent to an FE of only 4.7%) were observed. These results demonstrate that the photogenerated holes and electrons in the TiO_2 photoanode fully contributed to cellulose oxidation and spontaneous H_2 evolution, respectively. The photocurrent generated by the PEC cell gradually decreased, as distinct from the result described in Fig. 1b. This difference is attributed to the color of the cellulose solution gradually changing to light-yellow according to the progress of the PEC reaction as a result of the production of organic acids and to the photoanode being irradiated through the layer of the electrolyte during these gas analyses because of the limitation imposed by the gas-tight PEC cell configuration. (The change in color of the cellulose solution is discussed in detail later.) Indeed, the PEC cell could generate electricity and H_2 in a relatively stable manner (Fig. S18) when the two-chamber PEC cell (Fig. S4a) was used and the photoanode was irradiated from the glass-substrate side to avoid the harmful effect of light shielding by the colored electrolyte. In addition, irrespective of whether the purpose of the PEC cell is electric power generation or H_2 evolution, the PEC cell without cellulose generated only marginal photocurrent under the short-circuit condition compared with the cell that contained cellulose (Fig. S18). Therefore, the PEC complete decomposition of cellulose into CO_2 should indicate that the proposed PEC cell can convert almost all the Gibbs free energy contained in cellulose into electric power or H_2 with the assistance of photon energy.

3.3. Influence of the photoelectrode structure on the photoelectrochemical properties

One possible approach to improving the efficiency of the PEC cell is to use visible-light-responsive photoanodes, as previously mentioned. The other important aspect to improving PEC performance is to design a more suitable particulate photoelectrode structure. In the field of PEC water splitting, photoelectrodes consisting of a multilayer of stacked photocatalytic particles prepared by the squeegee method or by electrophoretic deposition sometimes exhibit limited PEC performance because of the resistance between the heavily stacked semiconductor particles. To improve the activities of such stacked photoelectrodes, specific methods such as a necking treatment are usually necessary [42–44]. Meanwhile, the PT method is well known as a versatile methodology to fabricate an efficient photoelectrode for PEC water splitting [22]. Because the PT photoelectrodes compose an approximate monolayer of photocatalytic particles directly anchored onto the backside metal layer, the photoelectrodes achieve favorable ohmic contact between the semiconductor particles and the backside electrode as well as reduced contact resistance between the stacked photocatalytic particles. For instance, an STO photoanode prepared by the PT method was found to exhibit high PEC activities for the OER under UV-light irradiation [45].

The current–potential curves of the TiO_2 stacked, STO stacked, TiO_2 PT, and STO PT photoanodes during the OER and the cellulose oxidation reaction are summarized in Fig. 4a and b, respectively. In the case of STO, the photoanode prepared by the PT method showed superior performance compared with the photoanode consisting of stacked photocatalytic particles, irrespective of whether the target reaction was the OER or the cellulose oxidation reaction. By contrast, the TiO_2 stacked photoanode generated a higher anodic photocurrent than the TiO_2 PT photoanode, irrespective of the target reaction. This opposite tendency between TiO_2 and STO might be attributable to the difference in their particle sizes. As shown in the SEM images (Fig. S19), the stacked photoanodes possessed a porous structure containing voids with sizes of several tens of nanometers, whereas the PT photoanodes possessed a monolithic structure consisting of an approximate monolayer of photocatalytic particles anchored to the metal layer. Notably, because of the extremely small particle sizes, the TiO_2 PT appears to be partially composed of stacked photocatalytic particles rather than

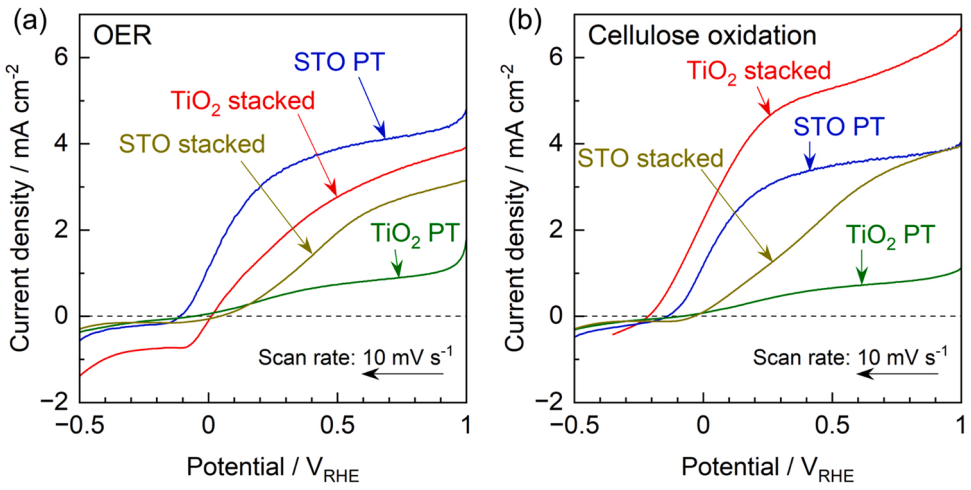

Fig. 4. Current–potential curves of TiO_2 stacked, STO stacked, TiO_2 PT, and STO PT photoanodes during (a) the OER using 2 M NaOH electrolyte without cellulose and (b) cellulose oxidation using the cellulose aqueous solution. A 300 W Xe lamp ($\lambda < 500$ nm) was used as a light source.

composed of a full monolayer. The particle sizes of the present TiO_2 and STO differed by one order of magnitude; specifically, the TiO_2 particles were several tens of nanometers, whereas the STO were several hundreds of nanometers. Therefore, the stacked photoanodes consisting of STO with relatively large particles might suffer from increased contact resistance because of the decreased numbers of junctions between the stacked STO particles per unit volume (this point will be discussed in the next paragraph). Meanwhile, the incomplete monolayer structure

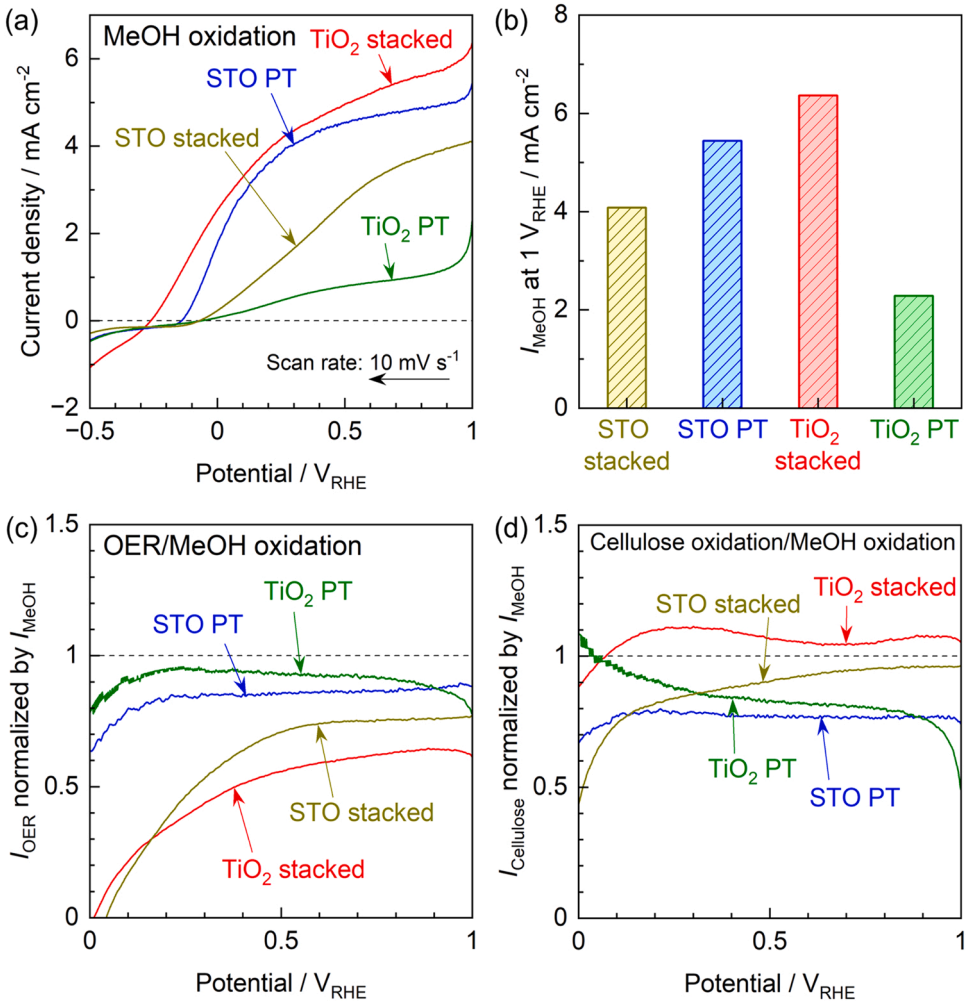

Fig. 5. (a) Current–potential curves of TiO_2 stacked, STO stacked, TiO_2 PT, and STO PT photoanodes in methanol aqueous solution, and (b) summary of the photocurrent generated during methanol oxidation at 1 V_{RHE}. (c and d) Potential dependence of the photocurrent ratio of (c) the OER and (d) cellulose oxidation to the photocurrent during methanol oxidation. A 300 W Xe lamp ($\lambda < 500$ nm) was used as a light source.

consisting of partially stacked small photocatalytic particles might be the origin of the inferior PEC performance of the TiO_2 PT. Another possibility is that an approximate monolayer of TiO_2 with a small particle size prepared by the PT method might be insufficient to absorb the incident photons. Indeed, the STO PT showed slightly greater absorption capability compared with the TiO_2 PT (Fig. S20). Nevertheless, we considered that the stacked structure should achieve efficient photoanode performance from relatively small photocatalytic particles (TiO_2 in the present case), whereas the PT method is likely preferable for manufacturing relatively large photocatalytic particles (STO in the present case). Here, we note that, to verify the general applicability of this conclusion, photoanodes consisting of different photocatalytic particles with different sizes should be examined. However, synthesizing photocatalytic particles that differ in particle size but exhibit otherwise identical physical characteristics is difficult. For instance, increasing the synthesis temperature should increase the average particle size but would likely also change the crystallinity and crystalline structure of the particles [46]. Thus, a more detailed investigation of the effects of particle size on the PEC performance using photocatalytic materials that differ only in particle size is left as a topic for a future study. During the PEC OER (Fig. 4a), the STO PT electrode showed substantial PEC performance compared with the TiO_2 stacked photoanode, which is reasonable given previous reports of highly efficient PT photoanodes for PEC water splitting [45,47,48]. However, we were surprised that the TiO_2 stacked photoanode exhibited a higher photocurrent than the STO PT photoanode during the cellulose oxidation reaction (Fig. 4b).

To further discuss these opposite tendencies during the PEC OER and cellulose oxidation reaction, the PEC performance during methanol oxidation was also assessed (Fig. 5a and b). In the current–potential curves of the Pt disk electrode during methanol oxidation, cellulose oxidation, and the OER (Fig. S21), the most negative onset potential was observed for methanol oxidation, whereas the most positive onset potential was observed for the OER. This trend implies that methanol oxidation should be the electrochemically easiest reaction, followed by cellulose oxidation, and that the OER should be the most challenging reaction. In addition, the concentration of methanol solution used in the present study was almost transparent in the UV-light region (Fig. S22) and was thus suitable as a sacrificial reagent for PEC reactions using UV-light-responsive STO or TiO_2. Therefore, an anodic photocurrent observed during decomposition of the sacrificial reagent (methanol in the present case) should reflect the "maximum" photocurrent for the present photoanode material and structure, where the surface reaction kinetics no longer limit the overall PEC reaction rate [49,50]. Here, a comparison of the photocurrent during methanol oxidation between stacked and PT photoanodes should reflect the "quality" of the prepared particulate photoanodes. Similar to the previous discussion regarding Fig. 4, during methanol oxidation, the STO PT photoanode showed a higher anodic photocurrent than the STO stacked photoanode, whereas the TiO_2 stacked photoanode showed a higher photocurrent than the TiO_2 PT photoanode (Fig. 5b). To further clarify the aforementioned difference in resistance of the TiO_2 stacked and STO stacked photoanodes, we compared the slope of their current–potential curves in the vicinity of the onset potential during methanol oxidation. In the field of PEC and photovoltaics, the slope of the current–voltage profile near the open-circuit condition is known to reflect the series resistance of the device and, thus, to directly affect the fill factor [51–53]. The current–potential curves and the corresponding differential curves are compiled in Fig. S23. In the present case, the TiO_2 stacked photoanode actually showed a substantially larger slope near the onset potential (-0.2 to $0\ V_{RHE}$) compared with the STO stacked photoanode (0.1–$0.4\ V_{RHE}$), indicating a lower internal resistance of the TiO_2 stacked photoanode. These observations also support our inference that the appropriate fabrication method for particulate photoelectrodes should depend on the particle size of the photocatalytic particles used.

Next, we calculated the ratio of the photocurrent during the OER (I_{OER}) or cellulose oxidation reaction ($I_{cellulose}$) to that during the methanol oxidation reaction (I_{MeOH}) (Fig. 5c and 5d). The corresponding current–potential curves obtained using the individual photoanodes during methanol oxidation, cellulose oxidation, and the OER are summarized in Fig. S24. These ratios of I_{OER} or $I_{cellulose}$ to I_{MeOH} should function as indicators for determining whether the surface reaction kinetics of the OER or the cellulose oxidation reaction were sufficiently slow to limit the charge transfer from the photocatalysts to the reaction substrates. When this index is close to 1, the bottlenecks in the PEC reaction are attributable to physical processes inside the semiconductor (*e.g.*, photoexcitation, migration, and/or separation of photoexcited carriers) rather than to slow reaction kinetics. (Such indices are sometimes referred to as "charge injection efficiencies" in the literature [54–57].) When the particulate photoanodes were prepared by the PT method, irrespective of whether the photocatalyst was STO or TiO_2 and irrespective of whether the target reaction was the OER or cellulose oxidation reaction, the photocurrent ratios showed relatively large values close to 1 over a wide range of potentials (Fig. 5c and 5d). Thus, in the case of the PT photoanodes, the kinetics of the OER or the cellulose oxidation reaction no longer limit the overall PEC reaction rate and the photocurrent should be mainly determined by the charge separation inside the semiconductor particles. However, in the case of the stacked TiO_2 and STO photoanodes, the I_{OER}-to-I_{MeOH} ratios were relatively low; they gradually decreased according to the negative shift of the applied potential and finally reached approximately 0 at $\sim 0\ V_{RHE}$ (Fig. 5c). Nonetheless, the $I_{cellulose}$-to-I_{MeOH} ratios achieved by the stacked photoanodes equaled almost unity over a wide range of applied potentials (Fig. 5d). These observations indicate that slow reaction kinetics of the OER should limit the photocurrent achieved by the stacked photoanodes, whereas they can generate the "maximum" photocurrent expected for the present material and structure during cellulose oxidation.

The discussions thus far regarding the reaction pathway during PEC cellulose oxidation, as well as the influences of photoelectrode structure, can be summarized as follows (Fig. 6). The PEC oxidation of cellulose dissolved in an aqueous solution was initiated by the scission of cellulose chains, followed by gradual decomposition into relatively small hydrocarbons and finally into CO_2. This reaction mechanism is consistent with that reported for PEC decomposition of solid cellulose [8]. In a thermodynamically challenging reaction (*i.e.*, when the equilibrium potential is relatively positive) such as the OER, the monolithic structure of the PT photoanodes with a low electric resistance regarding back contact and stacked particles should be advantageous for attaining a high photocurrent. Meanwhile, to drive a thermodynamically easier but kinetically slow multielectron reaction such as cellulose oxidation, the high specific surface area of the stacked photoanodes should be preferable. Indeed, the TiO_2 stacked photoanode also exhibited a higher anodic photocurrent than the STO PT photoanode during methanol oxidation, which is a thermodynamically easier organic decomposition reaction (Fig. 5a and 5b). As an additional benefit, the structure of the TiO_2 stacked photoanode led to a stable anodic photocurrent during long-term PEC cellulose oxidation. As shown in Fig. S25, the anodic photocurrent generated by the PT photoanode during cellulose oxidation completely disappeared within 60 min of light irradiation despite the cellulose solution being used as a fuel, as distinct from the case of the TiO_2 stacked photoanode (Fig. 1b). This decrease of the photocurrent is attributable to the change in color of the cellulose solution during the PEC reaction (Fig. S26). The cellulose solution became light-yellow because of the generation of intermediate organic acids, which exhibited strong absorption in the UV–vis light region and thus interfered with the photoexcitation of the photocatalysts. Stacked photoanodes composing a transparent conductive substrate have often been used in PEC cells that contain a colored electrolyte (*e.g.*, dye-sensitized solar cells [58]) because such photoelectrodes can be irradiated from the glass-substrate side and the color of the electrolyte therefore barely inhibits the photoexcitation of the light absorber. For cellulose oxidation as well, the present cell configuration in which the stacked photoanode

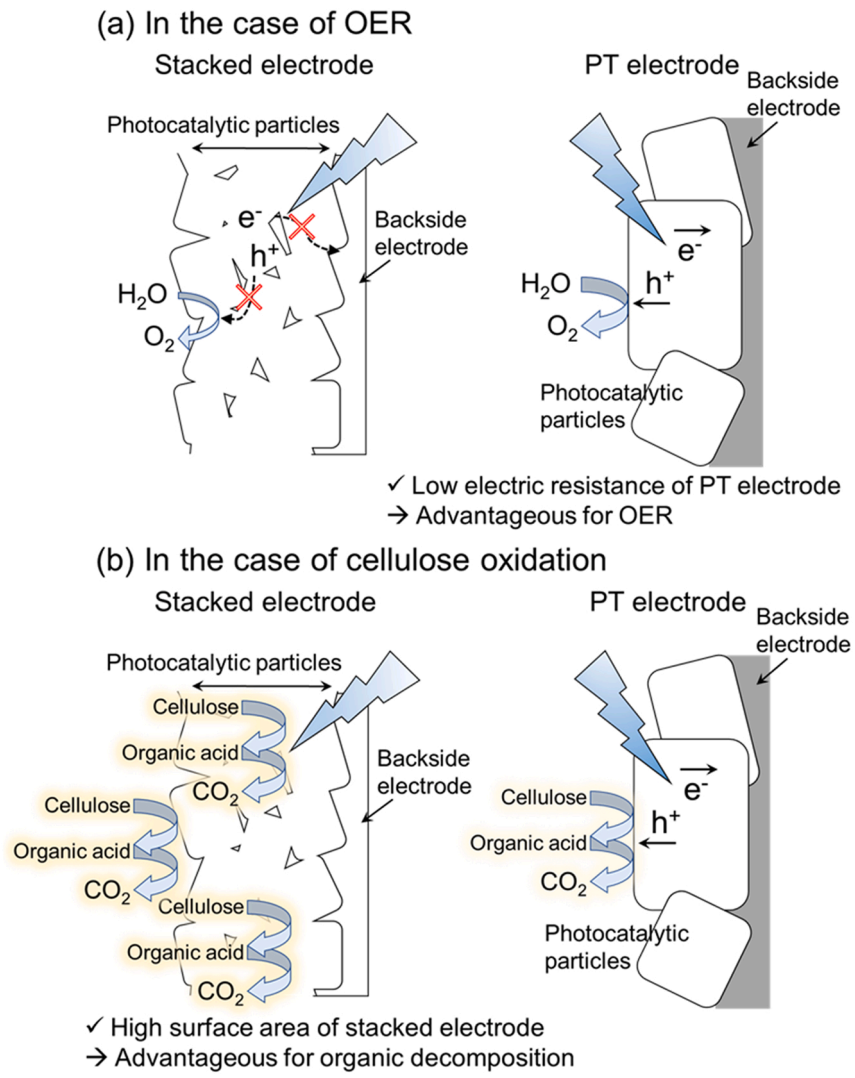

Fig. 6. Schematics of the influences of the photoelectrode structures on the PEC performance during (a) the OER and (b) cellulose oxidation.

itself was settled as a window should be advantageous to avoid the harmful light-shielding effects of the colored electrolyte containing the intermediate organic acids.

4. Conclusion

A PEC cell for electric power generation or H_2 evolution from a cellulose aqueous solution was constructed. The PEC cell employing a cellulose solution as a liquid fuel stably generated a photocurrent over a period of several hours because of the continuous supply of reactant to the photoanode from the bulk electrolyte. By contrast, the photocurrent obtained by the photoanode loaded with solid cellulose immediately degraded because of the rapid consumption of the available solid fuel. The PEC cell consisting of the TiO_2 stacked photoanode and a Pt-based cathode demonstrated spontaneous H_2 evolution from a cellulose solution without any external bias voltage under one-step photoexcitation of TiO_2. During the PEC reaction, relatively low-molecular-weight organic acids (*i.e.*, succinic acid, glyceric acid, malonic acid, glycolic acid, and formic acid) were gradually generated. In addition, the concentration of CO_2 dissolved in the strongly alkaline cellulose solution also increased according to the progress of the PEC reaction, although substantial O_2 was not evolved. Therefore, we concluded that almost all of the photogenerated holes in the photoanode are likely involved in cellulose oxidation, where cellulose dissolved in an aqueous solution is first cleaved into relatively small hydrocarbons and finally decomposed into CO_2. The stacked and PT photoanodes consisting of TiO_2 and STO photocatalytic particles were also comprehensively compared during the OER, methanol oxidation, and cellulose oxidation reactions. Judging from the ratios between the I_{OER} or $I_{cellulose}$ and $I_{methanol}$, irrespective of whether the PT photoanodes were undergoing OER or cellulose oxidation, the obtained photocurrent was mainly dominated by the physical processes inside the photocatalytic particles rather than by the surface reaction kinetics. The stacked photoanodes could also generate the "maximum" photocurrent without being limited by the surface reaction kinetics when driving cellulose oxidation, although the kinetics of the OER substantially affected the PEC performance. Overall, the monolithic structure of the STO PT photoanodes provided a high photocurrent during the OER because of the low electric resistance, whereas the TiO_2 stacked photoanode was suitable for high performance during cellulose decomposition because of the high specific surface area of the TiO_2 particles. This study emphasizes the superiority of using a cellulose solution as a liquid fuel rather than solid cellulose in future implementations of the direct energy utilization of waste biomass.

Declaration of Competing Interest

The authors declare the following financial interests/personal relationships which may be considered as potential competing interests:

Yosuke Kageshima, Hiromasa Nishikiori reports financial support was provided by Japan Society for the Promotion of Science.

Data availability

Data will be made available on request.

Acknowledgements

This study was financially supported by a Grant-in-Aid for Scientific Research (B) (no. 21H01715) from the Japan Society for the Promotion of Science (JSPS). This study was also funded in part by a Grant-in-Aid for Scientific Research (C) (no. 22K05297).

Appendix A. Supporting information

Supplementary data associated with this article can be found in the online version at doi:10.1016/j.apcatb.2023.122431.

References

[1] L.J.R. Nunes, T.P. Causer, D. Ciolkosz, Biomass for energy: a review on supply chain management models, Renew. Sustain. Energy Rev. 120 (2020), 109658, https://doi.org/10.1016/j.rser.2019.109658.
[2] A.C. Caputo, M. Palumbo, P.M. Pelagagge, F. Scacchia, Economics of biomass energy utilization in combustion and gasification plants: effects of logistic variables, Biomass-.-. Bioenergy 28 (2005) 35–51, https://doi.org/10.1016/j.biombioe.2004.04.009.
[3] P. McKendry, Energy production from biomass (part 1): overview of biomass, Bioresour. Technol. 83 (2002) 37–46, https://doi.org/10.1016/S0960-8524(01)00118-3.
[4] C. Li, S.B. Naghadeh, L. Guo, K. Xu, J.Z. Zhang, H. Wang, Cellulose as sacrificial biomass for photocatalytic hydrogen evolution over one-dimensional CdS loaded with NiS_2 as a cocatalyst, ChemistrySelect 5 (2022) 1470–1477, https://doi.org/10.1002/slct.201904840.
[5] H. Nagakawa, M. Nagata, Highly efficient hydrogen production in the photoreforming of lignocellulosic biomass catalyzed by Cu,In-doped ZnS derived from ZIF-8, Adv. Mater. Interfaces 9 (2022) 2101581, https://doi.org/10.1002/admi.202101581.
[6] D.B. Nimbalkar, V.-C. Nguyen, C.-Y. Shih, H. Teng, Melem-derived poly(heptazine imide) for effective charge transport and photocatalytic reforming of cellulose into H_2 and biochemicals under visible light, Appl. Catal. B 316 (2022), 121601, https://doi.org/10.1016/j.apcatb.2022.121601.
[7] V.-C. Nguyen, D.B. Nimbalkar, L.D. Nam, Y.-L. Lee, H. Teng, Photocatalytic cellulose reforming for H_2 and formate production by using graphene oxide-dot catalysts, ACS Catal. 11 (2021) 4955–4967, https://doi.org/10.1021/acscatal.1c00217.
[8] Y. Kageshima, T. Yoshimura, S. Koh, M. Mizuno, K. Teshima, H. Nishikiori, photoelectrochemical complete decomposition of cellulose for electric power generation, ChemCatChem 13 (2021) 1530–1537, https://doi.org/10.1002/cctc.202001665.
[9] H. Hao, L. Zhang, W. Wang, S. Zeng, Facile modification of titania with nickel sulfide and sulfate species for the photoreformation of cellulose into hydrogen, ChemSusChem 11 (2018) 2810–2817, https://doi.org/10.1002/cssc.201800743.
[10] A. Caravaca, W. Jones, C. Hardacre, M. Bowker, H_2 production by the photocatalytic reforming of cellulose and raw biomass using Ni, Pd, Pt and Au on titania, Proc. R. Soc. A 472 (2016) 20160054, https://doi.org/10.1098/rspa.2016.0054.
[11] G. Zhang, C. Ni, X. Huang, A. Welgamage, L.A. Lawton, P.K.J. Robertson, J.T. S. Irvine, Simultaneous cellulose conversion and hydrogen production assisted by cellulose decomposition under UV-light photocatalysis, Chem. Commun. 52 (2016) 1673–1676, https://doi.org/10.1039/C5CC09075J.
[12] A. Speltini, M. Sturini, D. Dondi, E. Annovazzi, F. Maraschi, V. Caratto, A. Profumo, A. Buttafava, Sunlight-promoted photocatalytic hydrogen gas evolution from water-suspended cellulose: a systematic study, Photochem. Photobiol. Sci. 13 (2014) 1410–1419, https://doi.org/10.1039/c4pp00128a.
[13] Z. Wang, Y. Guo, M. Liu, X. Liu, H. Zhang, W. Jiang, P. Wang, Z. Zheng, Y. Liu, H. Cheng, Y. Dai, Z. Wang, B. Huang, Boosting H_2 production from $BiVO_4$ photoelectrochemical biomass fuel cell by the construction of a bridge for charge and energy transfer, Adv. Mater. 34 (2022) 2201594, https://doi.org/10.1002/adma.202201594.
[14] L. He, Q. Liu, S. Zhang, X. Zhang, C. Gong, H. Shu, G. Wang, H. Liu, S. Wen, B. Zhang, High sensitivity of TiO_2 nanorod array electrode for photoelectrochemical glucose sensor and its photo fuel cell application, Electrochem. Commun. 94 (2018) 18–22, https://doi.org/10.1016/j.elecom.2018.07.021.
[15] L. Yan, Z. Gao, Dissolving of cellulose in PEG/NaOH aqueous solution, Cellulose 15 (2008) 789–796, https://doi.org/10.1007/s10570-008-9233-5.
[16] J. Cai, L. Zhang, Rapid dissolution of cellulose in LiOH/urea and NaOH/urea aqueous solutions, Macromol. Biosci. 5 (2005) 539–548, https://doi.org/10.1002/mabi.200400222.
[17] A. Isogai, R.H. Atalla, Dissolution of cellulose in aqueous NaOH solutions, Cellulose 5 (1998) 309–319, https://doi.org/10.1023/A:1009272632367.
[18] Y. Kageshima, Y. Ojima, H. Wada, S. Koh, M. Mizuno, K. Teshima, H. Nishikiori, Insights into the electrocatalytic oxidation of cellulose in solution toward applications in direct cellulose fuel cells, J. Phys. Chem. C. 125 (2021) 14576–14582, https://doi.org/10.1021/acs.jpcc.1c04357.
[19] M. Hao, X. Liu, M. Feng, P. Zhang, G. Wang, Generating power from cellulose in an alkaline fuel cell enhanced by methyl viologen as an electron-transfer catalyst, J. Power Sources 251 (2014) 222–228, https://doi.org/10.1016/j.jpowsour.2013.11.013.
[20] Y. Sugano, M. Vestergaard, H. Yoshikawa, M. Saito, E. Tamiya, Direct electrochemical oxidation of cellulose: a cellulose-based fuel cell system, Electroanalysis 22 (2010) 1688–1694, https://doi.org/10.1002/elan.201000045.
[21] H. Fan, G. Li, F. Yang, L. Yang, S. Zhang, Photodegradation of cellulose under UV light catalysed by TiO_2, J. Chem. Technol. Biotechnol. 86 (2011) 1107–1112, https://doi.org/10.1002/jctb.2632.
[22] T. Minegishi, N. Nishimura, J. Kubota, K. Domen, Photoelectrochemical properties of $LaTiO_2N$ electrodes prepared by particle transfer for sunlight-driven water splitting, Chem. Sci. 4 (2013) 1120–1124, https://doi.org/10.1039/C2SC21845C.
[23] Y. Ono, T. Ishida, H. Soeta, T. Saito, A. Isogai, Reliable d*n*/d*c* values of cellulose, chitin, and cellulose triacetate dissolved in LiCl/*N*,*N*-dimethylacetamide for molecular mass analysis, Biomacromolecules 17 (2016) 192–199, https://doi.org/10.1021/acs.biomac.5b01302.
[24] A.-L. Dupont, G. Harrison, Conformation and d*n*/d*c* determination of cellulose in *N*,*N*-dimethylacetamide containing lithium chloride, Carbohydr. Polym. 58 (2004) 233–243, https://doi.org/10.1016/j.carbpol.2004.07.016.
[25] Y. Kageshima, T. Kawanishi, D. Saeki, K. Teshima, K. Domen, H. Nishikiori, Boosted hydrogen-evolution kinetics over particulate lanthanum and rhodium-doped strontium titanate photocatalysts modified with phosphonate groups, Angew. Chem. Int. Ed. 60 (2021) 3654–3660, https://doi.org/10.1002/anie.202011705.
[26] Q. Wang, T. Hisatomi, S.S.K. Ma, Y. Li, K. Domen, Core/shell structured La- and Rh-codoped $SrTiO_3$ as a hydrogen evolution photocatalyst in Z-scheme overall water splitting under visible light irradiation, Chem. Mater. 26 (2014) 4144–4150, https://doi.org/10.1021/cm5011983.
[27] S. Ponnada, M.S. Kiai, D.B. Gorle, A. Nowduri, R.K. Sharma, Insight into the role and strategies of metal–organic frameworks in direct methanol fuel cells: a review, Energy Fuels 35 (2021) 15265–15284, https://doi.org/10.1021/acs.energyfuels.1c02010.
[28] Z.A.C. Ramli, S.K. Kamarudin, S. Basri, A.M. Zainoodin, The potential of novel carbon nanocages as a carbon support for an enhanced methanol electro-oxidation reaction in a direct methanol fuel cell, Int. J. Energy Res. 44 (2020) 10071–10086, https://doi.org/10.1002/er.5621.
[29] H.F. Fard, M. Khodaverdi, F. Pourfayaz, M.H. Ahmadi, Application of N-doped carbon nanotube-supported Pt-Ru as electrocatalyst layer in passive direct methanol fuel cell, Int. J. Hydrog. Energy 45 (2020) 25307–25316, https://doi.org/10.1016/j.ijhydene.2020.06.254.
[30] C.L. Vecchio, A. Serov, H. Romero, A. Lubers, B. Zulevi, A.S. Aricò, V. Baglio, Commercial platinum group metal-free cathodic electrocatalysts for highly performed direct methanol fuel cell applications, J. Power Sources 437 (2019), 226948, https://doi.org/10.1016/j.jpowsour.2019.226948.
[31] N. Kariya, A. Fukuoka, M. Ichikawa, Direct PEM fuel cell using "organic chemical hydrides'' with zero-CO_2 emission and low-crossover, Phys. Chem. Chem. Phys. 8 (2006) 1724–1730, https://doi.org/10.1039/B518369C.
[32] C. Zhang, X. Shen, Y. Pan, Z. Peng, A review of Pt-based electrocatalysts for oxygen reduction reaction, Front. Energy 11 (2017) 268–285, https://doi.org/10.1007/s11708-017-0466-6.
[33] Q.-Y. Liu, P. Wang, F.-G. Zhang, Y.-J. Yuan, Visible-light-driven photocatalytic cellulose-to-H_2 conversion by $MoS_2/ZnIn_2S_4$ photocatalyst with cellulase assistance, ChemPhysChem (2022), e202200319, https://doi.org/10.1002/cphc.202200319.
[34] Z. Yang, M. Zhu, Y. Niu, E. Kozliak, B. Yao, Y. Zhang, C. Zhang, T. Qin, Y. Jia, Q. Li, A graphene-based coaxial fibrous photofuel cell powered by mine gas, Adv. Funct. Mater. 29 (2019) 1906813, https://doi.org/10.1002/adfm.201906813.
[35] D. Pan, S. Xiao, X. Chen, R. Li, Y. Cao, D. Zhang, S. Pu, Z. Li, G. Li, H. Li, Efficient photocatalytic fuel cell *via* simultaneous visible-photoelectrocatalytic degradation and electricity generation on a porous coral-like WO_3/W photoelectrode, Environ. Sci. Technol. 53 (2019) 3697–3706, https://doi.org/10.1021/acs.est.8b05685.
[36] K. Fujiwara, A. Akita, S. Kawano, M. Fujishima, H. Tada, Hydrogen peroxide-photofuel cell using TiO_2 photoanode, Electrochem. Commun. 84 (2017) 71–74, https://doi.org/10.1016/j.elecom.2017.10.008.
[37] Q. Chen, J. Li, X. Li, K. Huang, B. Zhou, W. Cai, W. Shangguan, Visible-light responsive photocatalytic fuel cell based on WO_3/W photoanode and Cu_2O/Cu photocathode for simultaneous wastewater treatment and electricity generation, Environ. Sci. Technol. 46 (2012) 11451–11458, https://doi.org/10.1021/es302651q.
[38] S.Y. Oh, D.I. Yoo, Y. Shin, G. Seo, FTIR analysis of cellulose treated with sodium hydroxide and carbon dioxide, Carbohydr. Res. 340 (2005) 417–428, https://doi.org/10.1016/j.carres.2004.11.027.
[39] R.T. O'Connor, E.F. DuPré, D. Mitcham, Applications of infrared absorption spectroscopy to investigations of cotton and modified cottons: Part I: physical and crystalline modifications and oxidation, Text. Res. J. 28 (1958) 382, https://doi.org/10.1177/004051755802800503.

[40] X. Colom, F. Carrillo, Crystallinity changes in lyocell and viscose-type fibres by caustic treatment, Eur. Polym. J. 38 (2002) 2225–2230, https://doi.org/10.1016/S0014-3057(02)00132-5.
[41] A.-A.M.A. Nada, S. Kamel, M. El-Sakhawy, Thermal behaviour and infrared spectroscopy of cellulose carbamates, Polym. Degrad. Stab. 70 (2000) 347–355, https://doi.org/10.1016/S0141-3910(00)00119-1.
[42] N. Zhang, H. Zheng, Y. Guo, J. Feng, Z. Li, Z. Zou, Design principles for construction of charge transport channels in particle-assembled water-splitting photoelectrodes, ACS Sustain. Chem. Eng. 7 (2019) 10509–10515, https://doi.org/10.1021/acssuschemeng.9b01067.
[43] S.S. Gujral, A.N. Simonov, M. Higashi, R. Abe, L. Spiccia, Optimization of titania post-necking treatment of TaON photoanodes to enhance water-oxidation activity under visible-light irradiation, ChemElectroChem 2 (2015) 1270–1278, https://doi.org/10.1002/celc.201500224.
[44] M. Higashi, K. Domen, R. Abe, Highly stable water splitting on oxynitride TaON photoanode system under visible light irradiation, J. Am. Chem. Soc. 134 (2012) 6968–6971, https://doi.org/10.1021/ja302059g.
[45] Y. Ham, T. Minegishi, T. Hisatomi, K. Domen, A $SrTiO_3$ photoanode prepared by the particle transfer method for oxygen evolution from water with high quantum efficiencies, Chem. Commun. 52 (2016) 5011–5014, https://doi.org/10.1039/C6CC00497K.
[46] A. Kudo, Y. Miseki, Heterogeneous photocatalyst materials for water splitting, Chem. Soc. Rev. 38 (2009) 253–278, https://doi.org/10.1039/B800489G.
[47] K. Ueda, T. Minegishi, J. Clune, M. Nakabayashi, T. Hisatomi, H. Nishiyama, M. Katayama, N. Shibata, J. Kubota, T. Yamada, K. Domen, Photoelectrochemical oxidation of water using $BaTaO_2N$ photoanodes prepared by particle transfer method, J. Am. Chem. Soc. 137 (2015) 2227–2230, https://doi.org/10.1021/ja5131879.
[48] J. Seo, T. Takata, M. Nakabayashi, T. Hisatomi, N. Shibata, T. Minegishi, K. Domen, Mg–Zr cosubstituted Ta_3N_5 photoanode for lower-onset-potential solar-driven photoelectrochemical water splitting, J. Am. Chem. Soc. 137 (2015) 12780–12783, https://doi.org/10.1021/jacs.5b08329.
[49] F. Takagi, S. Taguchi, Y. Kageshima, K. Teshima, K. Domen, H. Nishikiori, Accelerated photoelectrochemical oxygen evolution over a $BaTaO_2N$ photoanode modified with cobalt-phosphate-loaded TiO_2 nanoparticles, Appl. Phys. Lett. 119 (2021), 123902, https://doi.org/10.1063/5.0061729.
[50] Y. Kageshima, T. Fujita, F. Takagi, T. Minegishi, K. Teshima, K. Domen, Y. Amao, H. Nishikiori, Electrochemical evaluation for multiple functions of Pt-loaded TiO_2 nanoparticles deposited on a photocathode, ChemElectroChem 6 (2019) 4859–4866, https://doi.org/10.1002/celc.201901453.
[51] W. Yang, R.R. Prabhakar, J. Tan, S.D. Tilley, J. Moon, Strategies for enhancing the photocurrent, photovoltage, and stability of photoelectrodes for photoelectrochemical water splitting, Chem. Soc. Rev. 48 (2019) 4979–5015, https://doi.org/10.1039/C8CS00997J.
[52] J.D. Servaites, S. Yeganeh, T.J. Marks, M.A. Ratner, Efficiency enhancement in organic photovoltaic cells: consequences of optimizing series resistance, Adv. Funct. Mater. 20 (2010) 97–104, https://doi.org/10.1002/adfm.200901107.
[53] N. Koide, A. Islam, Y. Chiba, L. Han, Improvement of efficiency of dye-sensitized solar cells based on analysis of equivalent circuit, J. Photochem. Photobiol. A Chem. 182 (2006) 296–305, https://doi.org/10.1016/j.jphotochem.2006.04.030.
[54] J. Lin, Y. Yu, Z. Zhang, F. Gao, S. Liu, W. Wang, G. Li, A novel approach for achieving high-efficiency photoelectrochemical water oxidation in InGaN nanorods grown on Si System: MXene nanosheets as multifunctional interfacial modifier, Adv. Funct. Mater. 30 (2020) 1910479, https://doi.org/10.1002/adfm.201910479.
[55] U. Prasad, J. Prakash, S.K. Gupta, J. Zuniga, Y. Mao, B. Azeredo, A.N.M. Kannan, Enhanced photoelectrochemical water splitting with Er- and W-codoped bismuth vanadate with WO_3 heterojunction-based two-dimensional photoelectrode, ACS Appl. Mater. Interfaces 11 (2019) 19029–19039, https://doi.org/10.1021/acsami.9b00150.
[56] Y. Liu, Y. Guo, L.T. Schelhas, M. Li, J.W. Ager, Undoped and Ni-doped CoO_x surface modification of porous $BiVO_4$ photoelectrodes for water oxidation, J. Phys. Chem. C. 120 (2016) 23449–23457, https://doi.org/10.1021/acs.jpcc.6b08654.
[57] P. Yan, G. Liu, C. Ding, H. Han, J. Shi, Y. Gan, C. Li, Photoelectrochemical water splitting promoted with a disordered surface layer created by electrochemical reduction, ACS Appl. Mater. Interfaces 7 (2015) 3791–3796, https://doi.org/10.1021/am508738d.
[58] M.S. Ahmad, A.K. Pandey, N.A. Rahim, Advancements in the development of TiO_2 photoanodes and its fabrication methods for dye sensitized solar cell (DSSC) applications. A review, Renew. Sust. Energ. Rev. 77 (2017) 89–108, https://doi.org/10.1016/j.rser.2017.03.129.